

COMBINATION OF BODY-FITTED AND EMBEDDED GRIDS FOR EXTERNAL VEHICLE AERODYNAMICS

Ralf Tilch, Ali Tabbal, Ming Zhu, Friedhelm Decker and Rainald Löhner

ESI Group, Silic 303, 94588 Rungis Cedex, France,

Volkswagen AG, Vehicle Development CAE-Methods,

Letterbox 1537, D-38436 Wolfsburg, Germany,

CFD Center, Dept. of Computational and Data Science

M.S. 6A2, College of Science, George Mason University

Fairfax, VA 22030-4444, USA

Body-fitted and embedded mesh techniques are combined to obtain accurate external aerodynamic solutions for realistic car geometries with minimal user intervention. The key idea is to mesh with typical body-fitted RANS grids the external shape of the vehicle, which is smooth and requires detailed physical modeling. The underhood and undercarriage are treated as embedded surfaces. The flow in this region is massively separated, requiring LES runs and isotropic grids. This makes it a suitable candidate for embedded grids. Comparisons with body-fitted and experimental data for a typical car show that this approach can yield drag predictions with an error less than 5%. Thus, the present approach reduces turnaround times for complete car geometries to 1-2 days, without compromising accuracy.

I. INTRODUCTION

With the advent of robust, accurate flow solvers and abundant, pervasive computer resources, the task of defining quickly a flow domain and the required boundary conditions has become a key bottleneck for numerical simulations. For external vehicle aerodynamics, the car industry at present is contemplating turnaround times of 1-2 days for arbitrary configurations. For so-called body fitted grids, the surface definition must be water-tight, and any kind of geometrical singularity, as well as small angles, should be avoided in order to generate a mesh of high quality. This typically presents no problems for the main ‘shape’ of the car (the part visible to a streetside observer), but can be difficult to obtain in such a short time for the underhood and undercarriage of a typical car or truck. Experience indicates that even with sophisticated software toolkits, manual cleanup in most cases takes several days for a complete car. An alternative is to use grids that are not body-conforming, and simply ‘embed’ the triangulations of the wetted surfaces of the structures in them. Techniques of this kind are also known as immersed, embedded, fictitious domain or Cartesian methods. The treatment of points in the vicinity of the embedded CSD triangulations or CSD bodies is modified in such a way that the required kinetic or kinematic boundary conditions are properly imposed^{1, 7-10, 12, 14, 15, 23, 27, 28, 30-34, 40}. At first sight, the solution of high Reynolds-number flows with grids of this type seems improper. Indeed, for the external shape portion the surface is smooth, and the interplay of pressure gradient and viscous/advective terms is what decides if separation will occur. Therefore, for this portion of the vehicle, a highly detailed, body-fitted RANS is considered mandatory. However, for the underhood and undercarriage, many abrupt changes in curvature occur, the flow is massively separated, and

Copyright © 2007 by the Authors. Published by the American Institute of Aeronautics and Astronautics, Inc. with permission.

an LES run seems sufficient. For embedded grids, this presents no problem. We are therefore in a rather fortunate position: the region where the geometry is the ‘dirtiest’ happens to be the region where isotropic grids are sufficient, making this region a good candidate for embedded grids. The key idea is then to obtain, quickly, the external shape of the vehicle and grid it with typical body-fitted RANS grids. We remark that this portion of the surface is typically ‘clean’, i.e. a turnaround of 1-2 days is possible. The underhood and undercarriage, on the other hand, is then inserted into the RANS mesh generated for the external shape of the vehicle as an embedded surface. As such, it can have crossing faces (stemming, for example, from different parts of the undercarriage), and does not require elements of very high quality. A run is then conducted with the embedded mesh.

Naturally, the question arises as to how accurate the results of this combination of body-fitted and embedded-surface techniques are, and whether it can be used for daily production runs. To this end, a typical car was analyzed. The case was run with the same solver and code, exercising the body-fitted, as well as the combined body-fitted/embedded-surface options. Pressure, velocity, as well as integrated force data were compared. The remainder of the paper is organized as follows: Section 2 describes the overall methodology and algorithms used for blast-structure interaction calculations. Sections 3,4 detail the embedded-mesh and immersed-body techniques used. Section 5 shows the comparison of several relevant runs, and discusses the implications. Some conclusions and an outlook are given in Section 6.

II. METHODOLOGY

Any CFD run proceeds through the following stages:

- Pre-Processing
- Grid Generation
- Flow Solver
- Post-Processing

In the pre-processing phase, the data and boundary conditions are acquired and defined, the desired mesh size is specified and all run-time files are prepared.

A typical vehicle data-set with underhood and undercarriage is given as 30-80 independent parts, which overlap and intersect each other in various forms. The definition of a closed and clean domain takes a considerably amount of time. Therefore a library (QuickModeling) for the model assembly/ cleaning of discrete surfaces was developed. It includes automatic tools for stitching, intersection and mesh optimisation. The intersection functionality detects, splits and repatches the surfaces, and improves the intersection lines and the connected surface meshes in one step. Within this environment one is able to reduce the pre-processing time for the first closed domain to 1-3 days. An additional 3-8 days have to be added for the final mesh.

For an external vehicle flow simulation the geometrical complexity of the underhood/ undercarriage produces a complex, massively separated flow structure and reduces locally very much the need for a highly detailed, body-fitted RANS simulation. Therefore the embedded mesh technology is applied in this region which has the consequence that the overall model preparation time can be reduced by 80-90% .

The accurate and highly detailed body-fitted mesh-solution is generated by the mesher. The flow solver uses the fully integrated embedded surface technology to adapt automatically the boundary-conditions, fluxes and mass-matrices for a given set of embedded surfaces and without any change in the previously generated mesh. For the applications shown here, these tasks were carried out with PRE-FLOW^{TM37}, a general pre-processor that can read a variety of CAD formats, prepare the domains for CFD runs and specify the desired element size and shape in space. The necessary stitching, intersection and optimisation of the line- and surface discretisation were carried within the library QuikModeling, called by PRE-FLOWTM. The computational domain is then filled with tetrahedral elements of specified size by using PAM-GEN3DTM, which incorporates the advancing front technique^{16,19,36}. For the flow solver (PAM-FLOWTM), a fractional step, projection-type finite element solver³⁹ is used. Post-processing is carried out using POST-FLOW^{TM38}.

III. EMBEDDED MESH TECHNIQUES

In what follows, we denote by CSD faces the surface of the object that is embedded. We implicitly assume that this information is given by a triangulation, which typically is obtained from a CAD package via STL files.

Embedded grids are treated by imposing appropriate **kinematic boundary conditions** for the fluid nodes close to the embedded surfaces. Depending on the required order of accuracy and simplicity, a first or second-order (higher-order) scheme may be chosen to apply the kinematic boundary conditions. Figure 1 illustrates the basic difference between these approaches. Note that in both cases the treatment of infinitely thin surfaces with fluid on both sides (e.g. membranes) is straightforward.

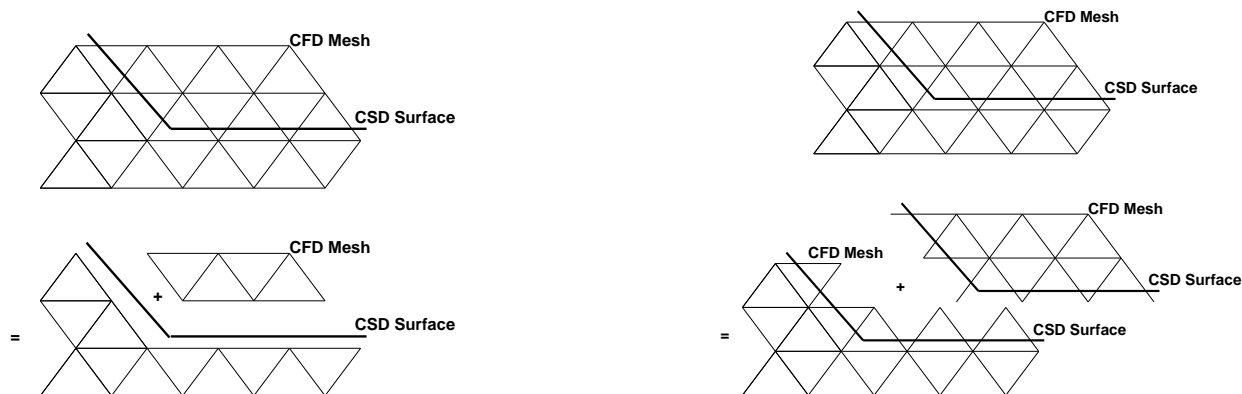


Figure 1: 1st/2nd Order Treatment of Embedded Surfaces

A first-order scheme may be achieved by:

- Eliminating the edges crossing the embedded surface;
- Forming boundary coefficients to achieve flux balance;
- Applying boundary conditions for the end-points of the crossed edges based on the normals of the embedded surface.

A second-order scheme may be obtained by:

- Duplicating the edges crossing the embedded surface;
- Duplicating the end-points of crossed edges;
- Applying boundary conditions for the end-points of the crossed edges based on the normals of the embedded surface.

Note that in either case CFD edges crossed by CSD faces are modified/duplicated. A number of fast algorithms have been developed to determine the edges crossed by the CSD faces, modify fluxes or mass-matrices close to the embedded surface, and to deactivate automatically the portions of the flow domain interior to a body^{23,25}. We therefore concentrate on the treatment of boundary conditions here.

3.1 First Order Treatment

For the new boundary points belonging to cut edges the proper PDE boundary conditions are required. For the cases considered here, these are given by an imposed velocity (Navier-Stokes) or an imposed normal velocity (Euler). For limiting and higher-order schemes, one may also have to impose boundary conditions on the gradients. The required surface normal and boundary velocity are obtained directly from the closest CSD face to each of the new boundary points.

These low-order boundary conditions may be improved by extrapolating the velocity from the surface with field information. The location where the flow velocity is equal to the surface velocity is the surface itself, and not the closest boundary point. As shown in Figure 2, for each boundary point the closest point on the CSD face is found. Then, two (three) neighbouring field (i.e., non-boundary) points are found and a

triangular (tetrahedral) element that contains the boundary point is formed. The velocity imposed at the field point is then found by interpolation. In this way, the boundary velocity ‘lags’ the field velocities by one timestep.

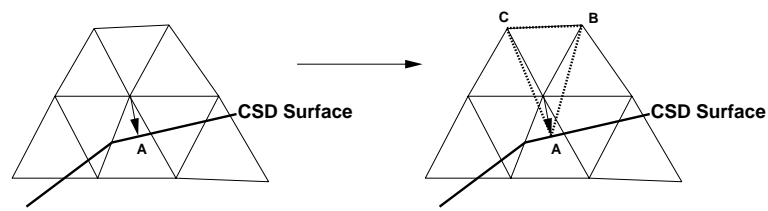


Figure 2: Extrapolation of Velocity

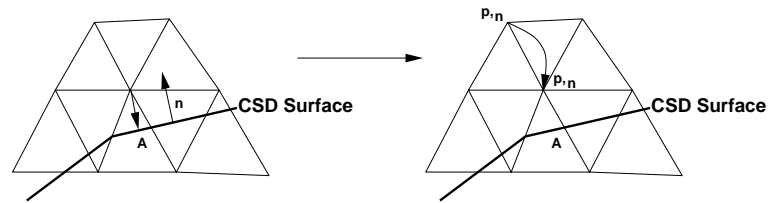


Figure 3: Extrapolation of Normal Pressure Gradient

The normal gradients at the boundary points can be improved by considering the ‘most aligned’ field (i.e., non-boundary) point to the line formed by the boundary point and the closest point on the CSD face (see Figure 3).

3.2 Higher Order Treatment

As stated before, a higher-order treatment of embedded surfaces may be achieved by using ghost points or mirrored points to compute the contribution of the crossed edges to the overall solution. This approach presents the advantage of not requiring the modification of the mass matrix as all edges (even the crossed ones) are taken into consideration. It also does not require an extensive modification of the various solvers. On the other hand, it requires more memory due to duplication of crossed edges and points, as well as (scalar) CPU time for renumbering/reordering arrays. Particularly for moving body problems, this may represent a considerable CPU burden. By duplicating the edges, the points are treated in the same way as in the original (non-embedded) case. The boundary conditions are imposed indirectly by mirroring and interpolating the unknowns as required. Figure 4 depicts the contribution due to the edges surrounding point i . A CSD boundary crosses the CFD domain. In this particular situation point j , which lies on the opposite side of the CSD face, will have to use the flow values of its mirror image j' based on the crossed CSD face.

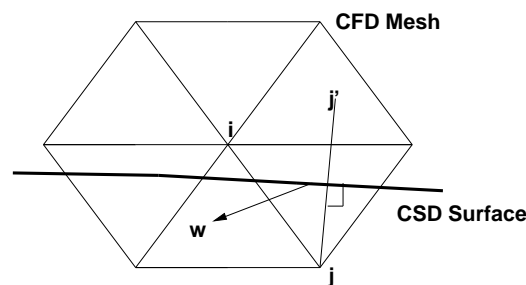


Figure 4: Higher Order Boundary Conditions

The element used for the interpolation might either be crossed (Figure 5a) or not exist (Figure 5b). In this case, the information interpolated is based solely on points that are truly inside the fluid domain, discarding the information of points that require interpolated information.

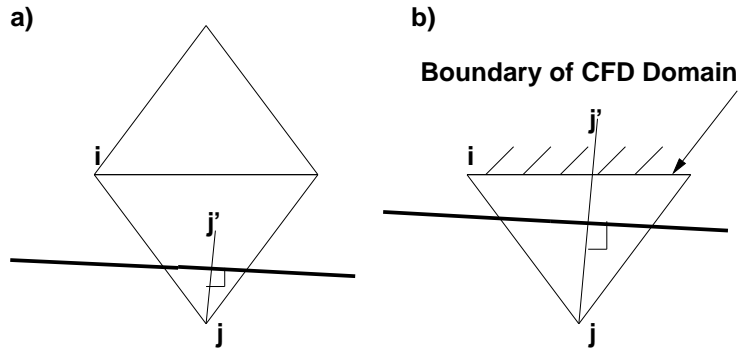


Figure 5: Problem Cases

Geometrically, this implies that the point at which the information is interpolated may not be located at the same normal distance from the wall as the point where information is required.

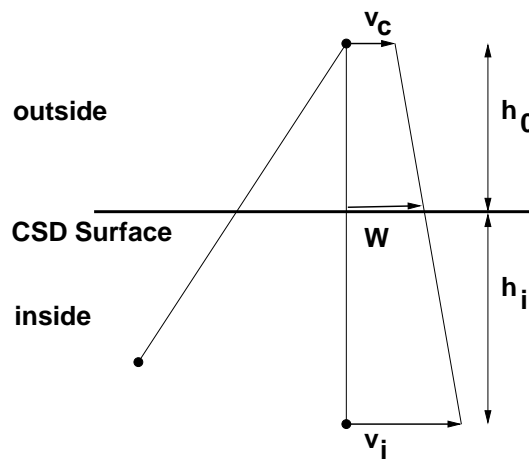


Figure 6: Navier-Stokes Boundary Condition

With the notation of Figure 6, and assuming a linear interpolation of the velocities, the values are interpolated as:

$$\mathbf{w} = (1 - \xi_w)\mathbf{v}_c + \xi_w\mathbf{v}_i \quad ; \quad \xi_w = \frac{h_o}{h_o + h_i} \quad , \quad (5)$$

i.e.

$$\mathbf{v}_c = \frac{1}{1 - \xi_w}\mathbf{w} - \frac{\xi_w}{1 - \xi_w}\mathbf{v}_i \quad . \quad (6)$$

Here \mathbf{w} is the average velocity of the crossed CSD face, \mathbf{v}_i the interpolated flow velocity and the distance factor $\xi_w \leq 0.5$.

IV. RESULTS

5.1 Flow Past a VW GOLF 5:

The case considered is shown in Figure 7. The starting point for this run was given by two NASTRAN-files which came from different departments at VW. The surface which was meshed using the body-fitted approach was given by 12 patches (one surface for the top, one for the bottom, two for the mirrors), whereas the surface which was treated with the embedded approach was given by 106 parts, most of which were single patches. The complete surface triangulation used to define the car had 1.1 Mtria. The body-fitted mesh consists of approximately 5.68 Mpts and 32.03 Mtets. Five RANS layers were used. For the car body,

the first point was $y_w = 0.758 \text{ mm}$ away from the wall, and the mesh was increased by a factor of $c_i = 1.5$ between layers. For the ground, the first point was $y_w = 0.914 \text{ mm}$ away from the ground, and the mesh was increased by a factor of $c_i = 1.4$ between layers. The surface of the body-fitted domain, the embedded surface, as well as the complete vehicle, are shown in Figures 7a-d. The distribution of element size in space may be discerned from Figures 7e-m. Note the boundary-layer mesh for the external shape, as well as the ground. A closeup of the undercarriage, together with the mesh in a cut plane, is shown in Figures 7j. The physical parameters were set as follows: $\mathbf{v}_\infty = (33.33, 0, 0) \text{ m/sec}$, $\rho = 1.2 \text{ kg/m}^3$, $\mu = 1.4 \cdot 10^{-5} \text{ kg/m}$, yielding a Reynolds-number of approximately $Re = 10^7$. A Smagorinsky turbulence model was used. The run was initialized with approximately 10^3 timesteps using local timesteps. This was followed by a time-accurate run of 10^4 timesteps, integrating explicitly the advective terms in order to obtain an accurate wake. The results obtained are shown in Figures 7n-p.



Figures 7a,b VW GOLF 5: Surface Grids (Body Fitted, Embedded)

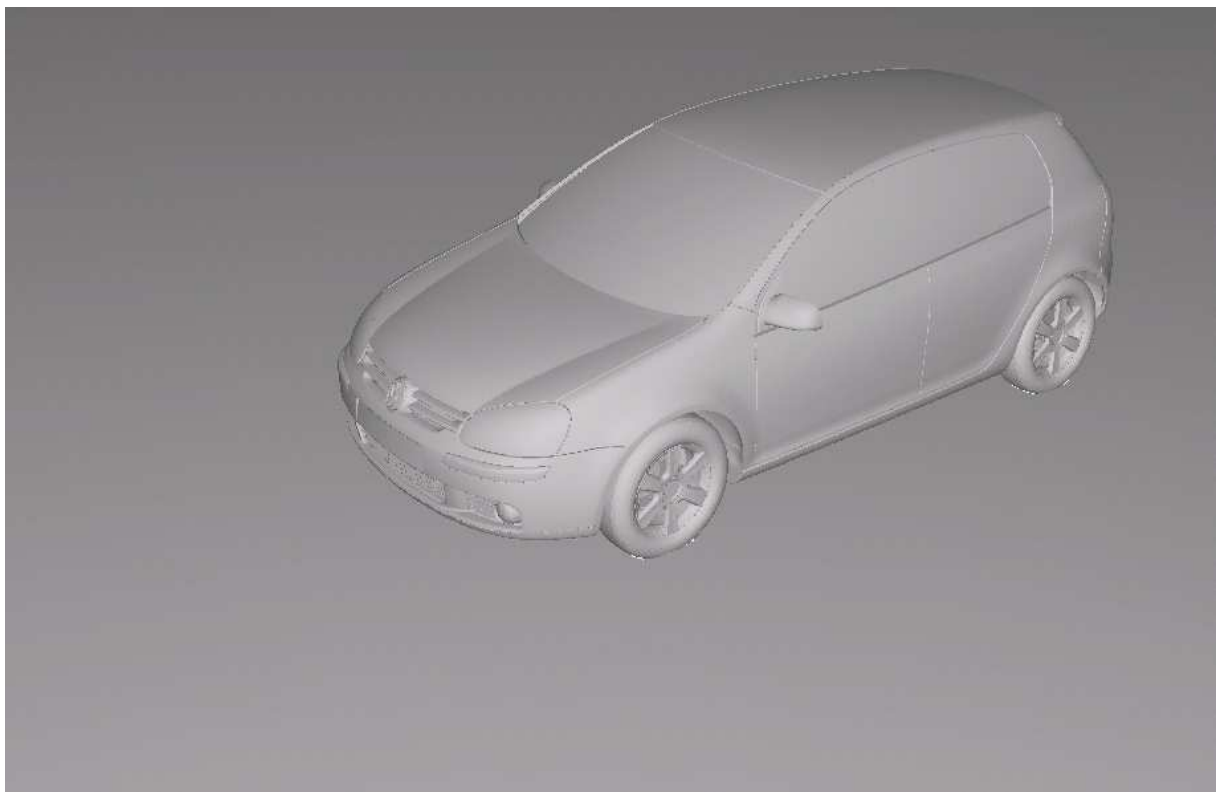


Figure 7c VW GOLF 5: Surface Grid (Body Fitted and Embedded)

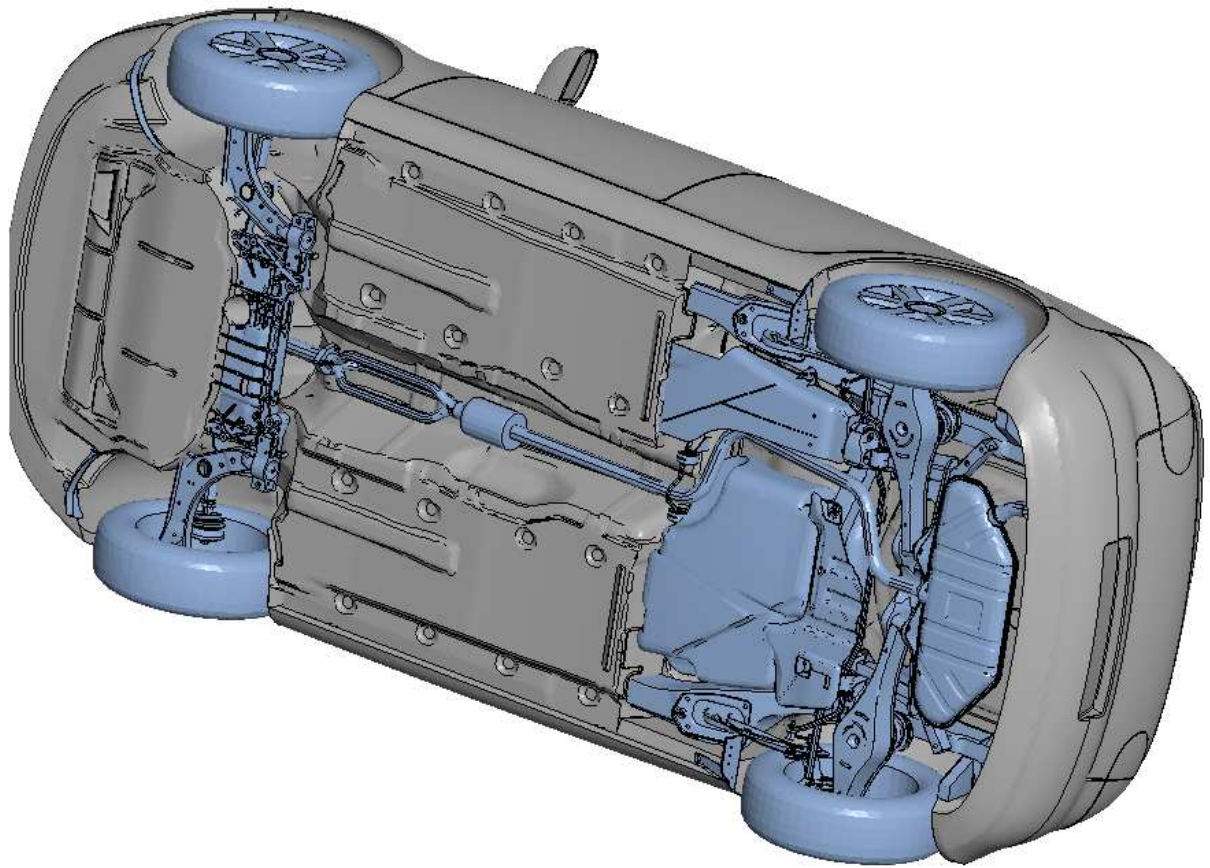


Figure 7d VW GOLF 5: View from Below (Body Fitted and Embedded)

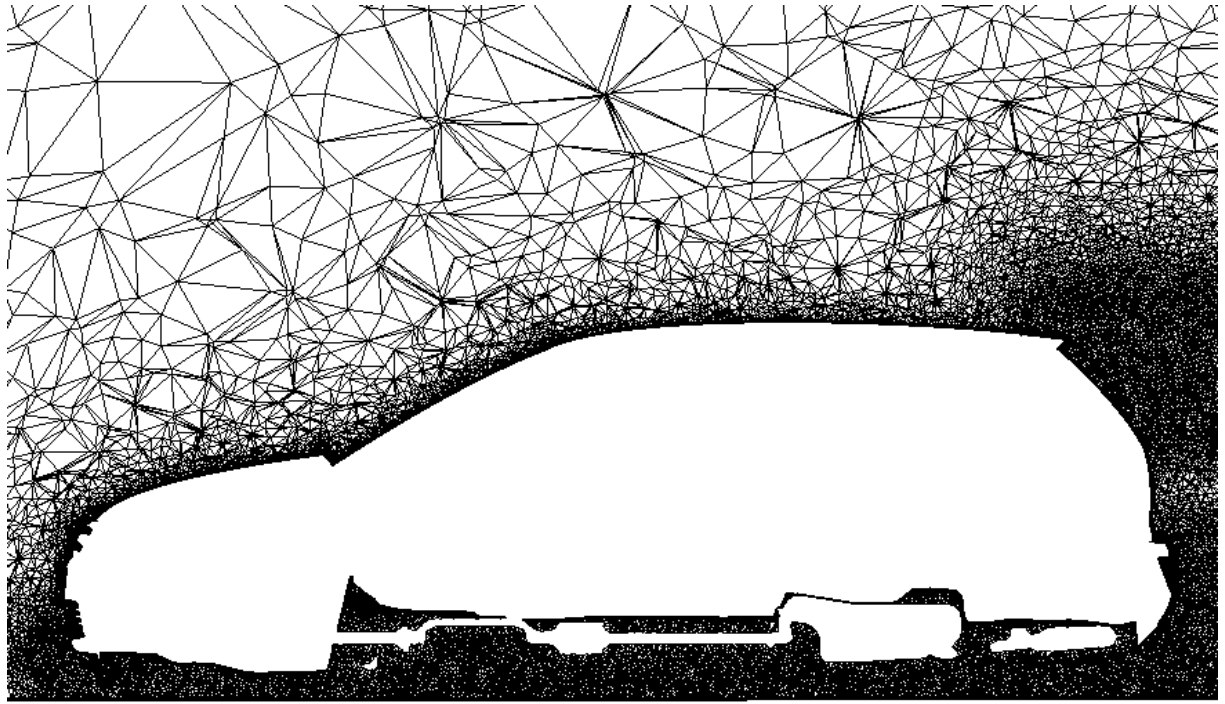
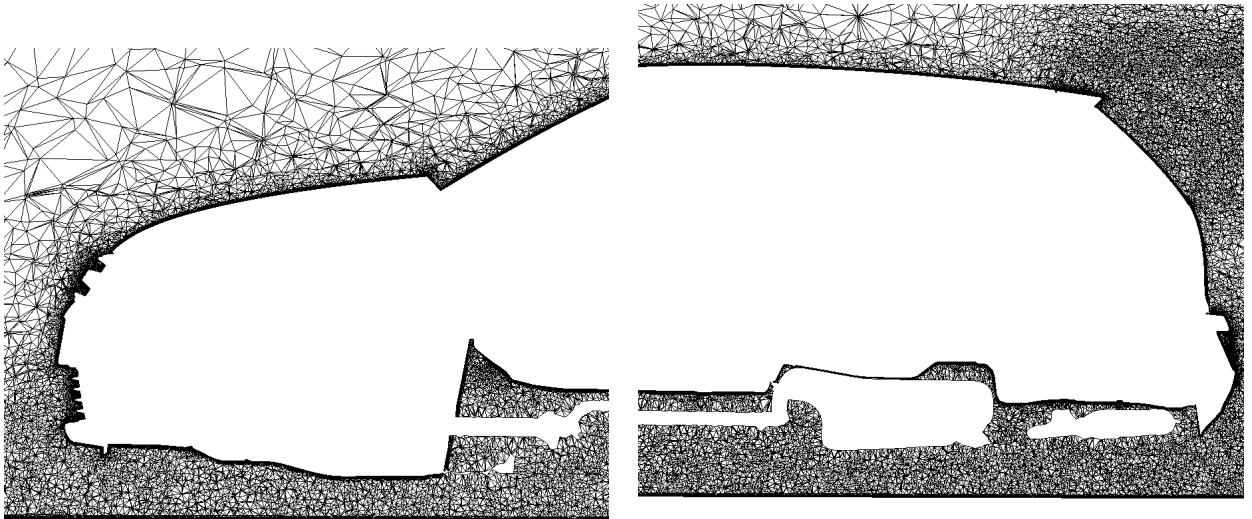


Figure 7e Cut Mesh in Mid-Plane



Figures 7h,i Cut Mesh in Mid-Plane (Detail)

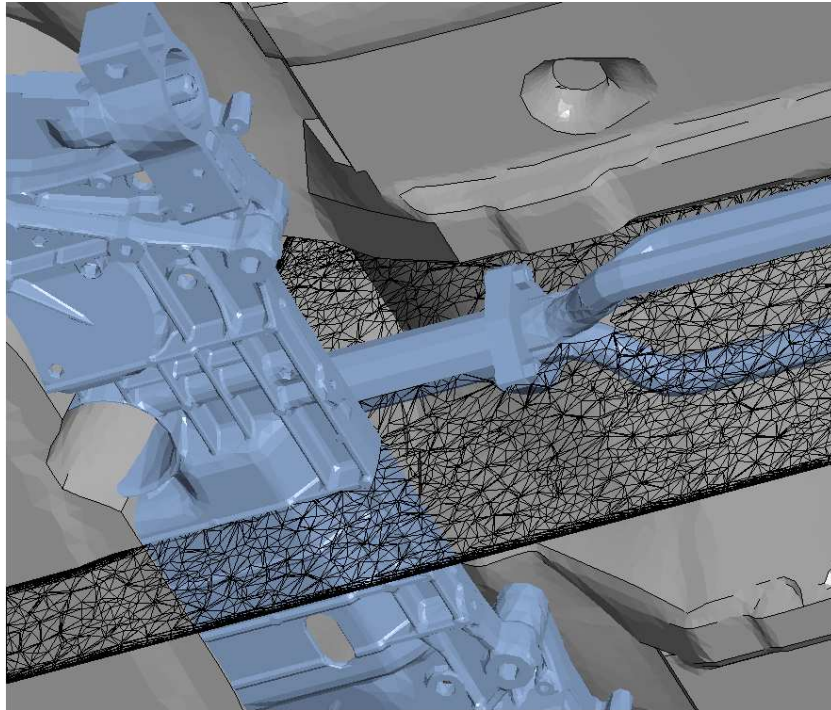


Figure 7j Undercarriage Detail

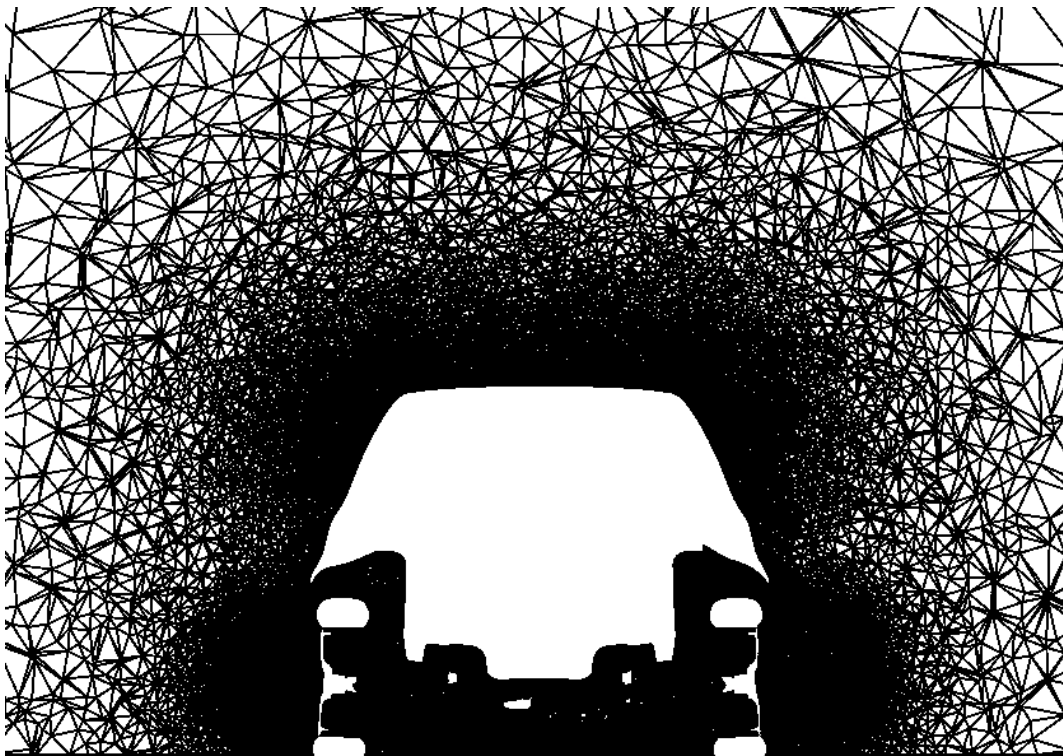


Figure 7k Cut in x-Plane

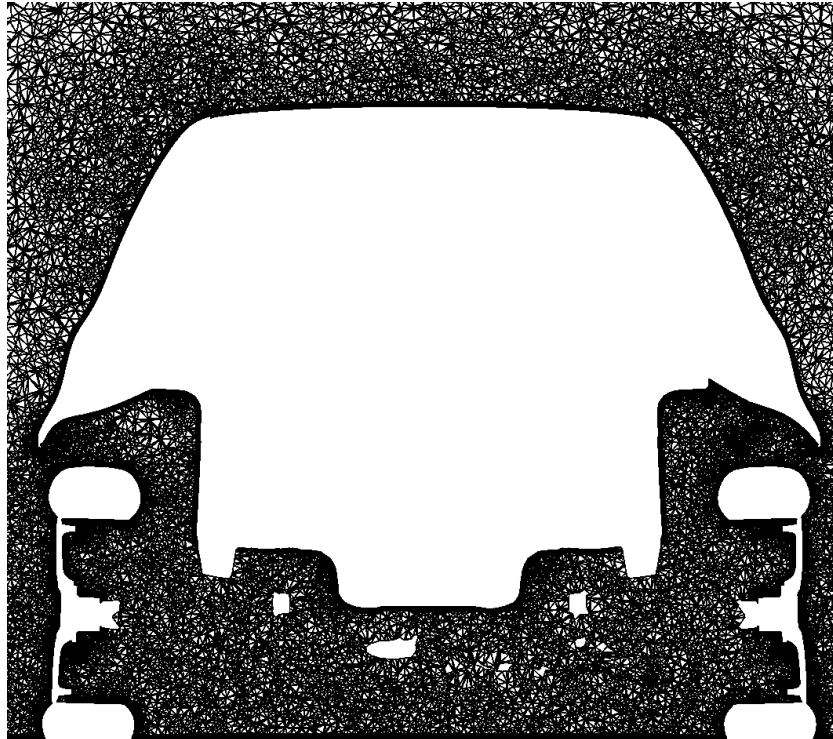


Figure 7l Cut in x-Plane: Detail

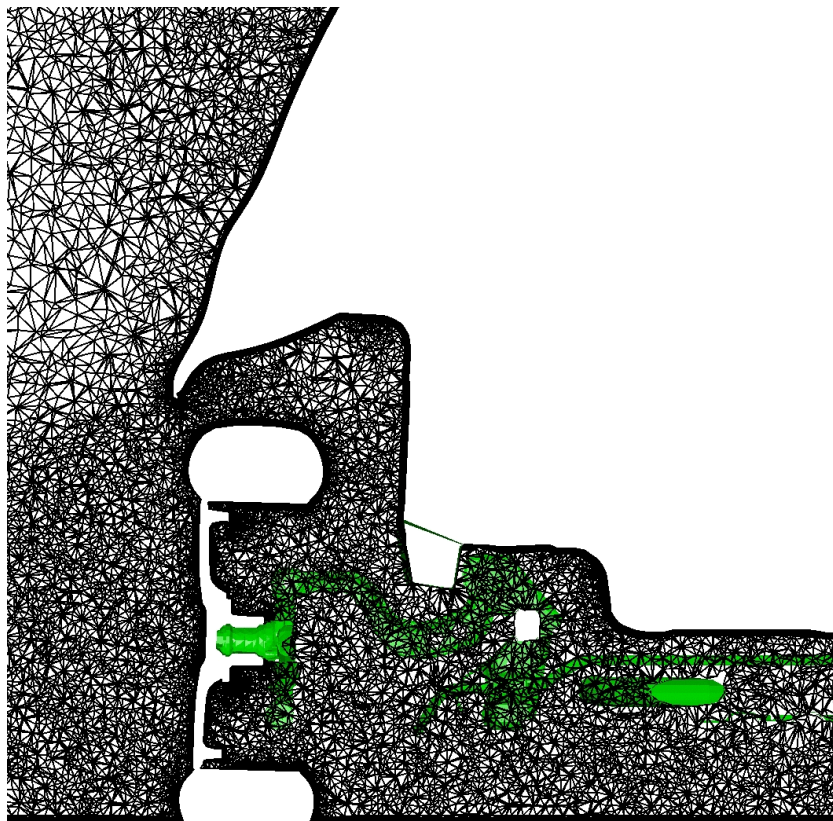


Figure 7m Cut in x-Plane: Detail

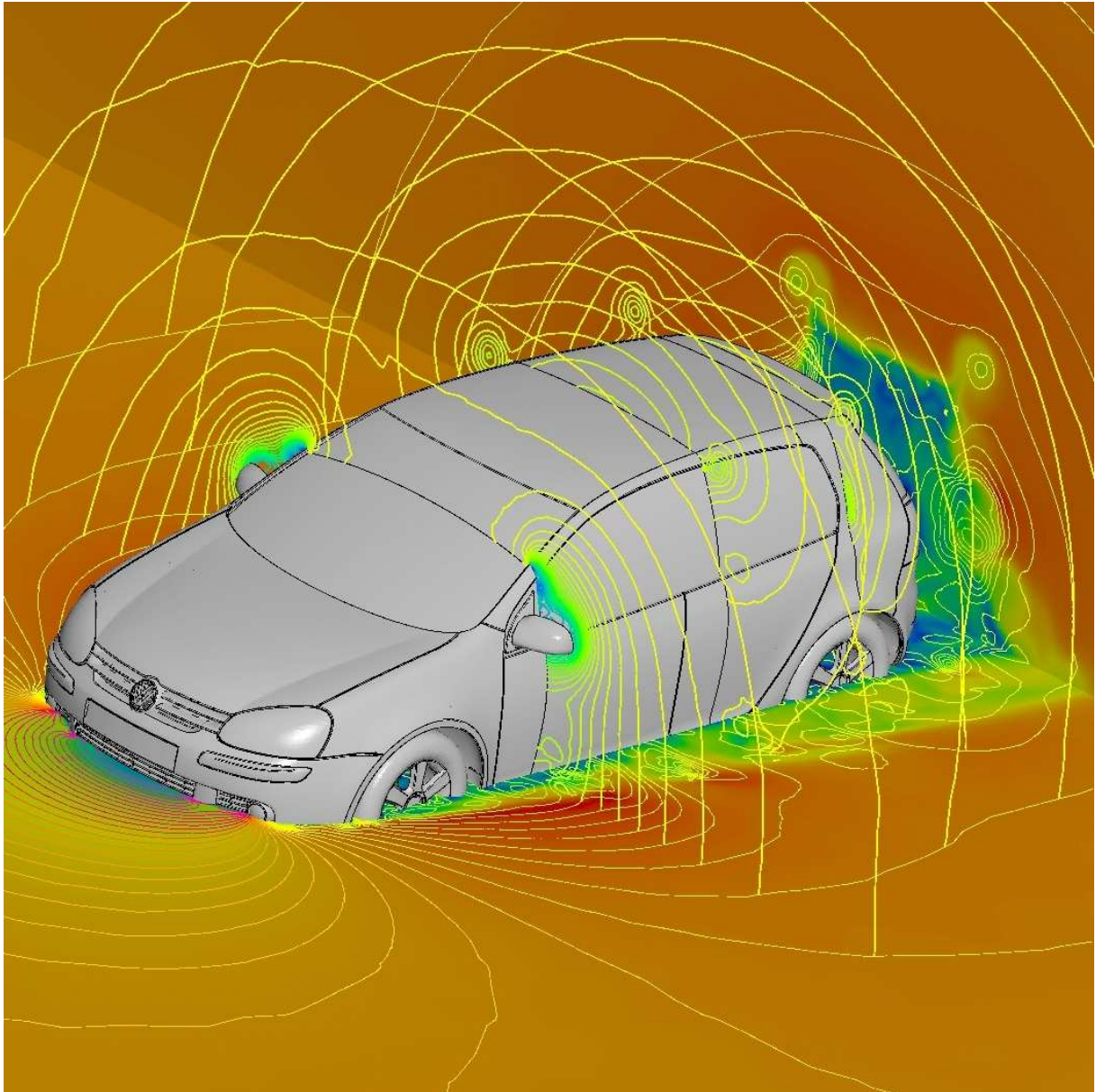


Figure 7n Pressure (Contours) on y-Plane and x-Planes, Velocity (Shaded) in y-Plane and back x-Plane

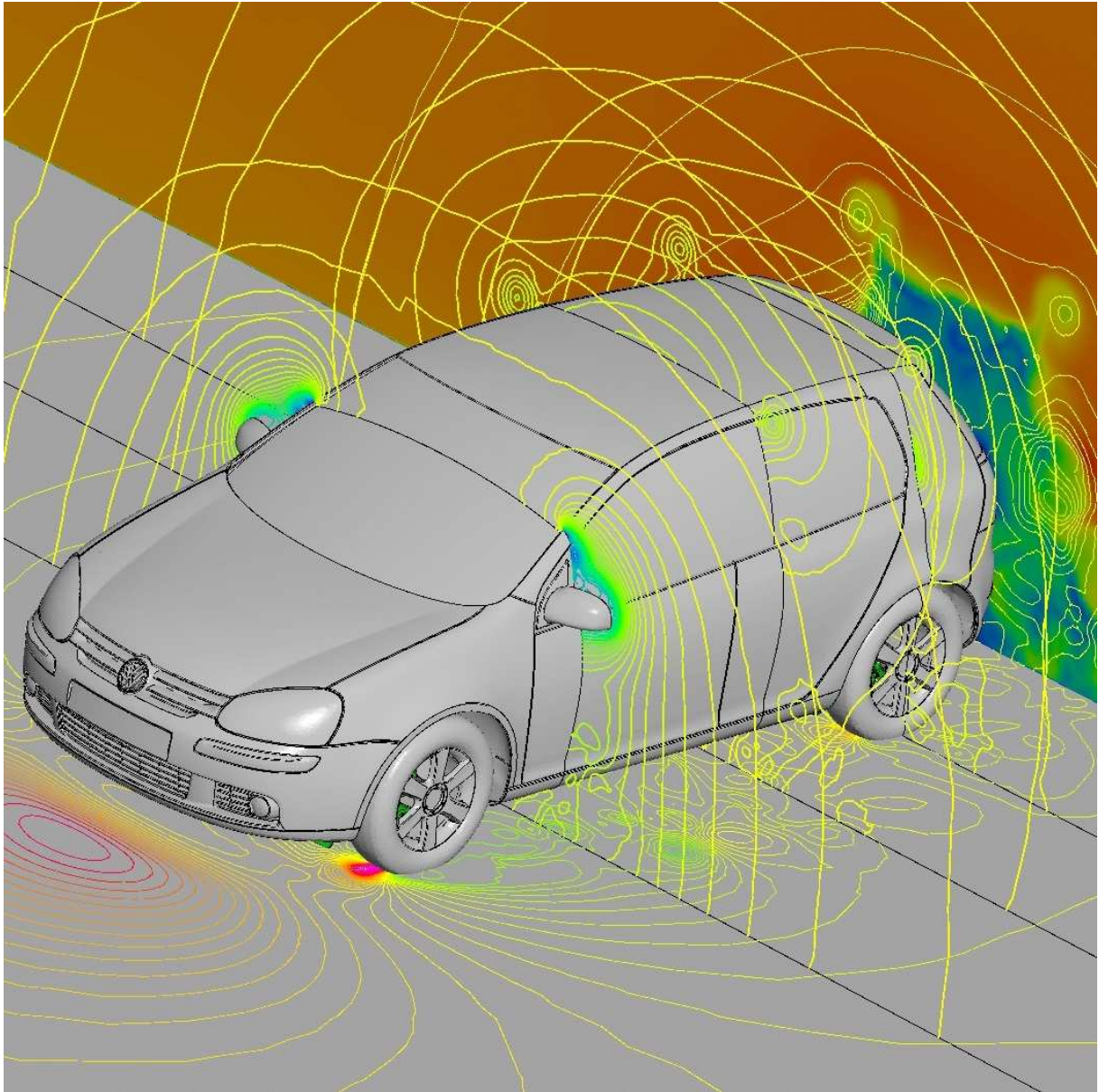


Figure 7o Pressure (Contours) on Ground and x-Planes, Velocity (Shaded) in back x-Plane

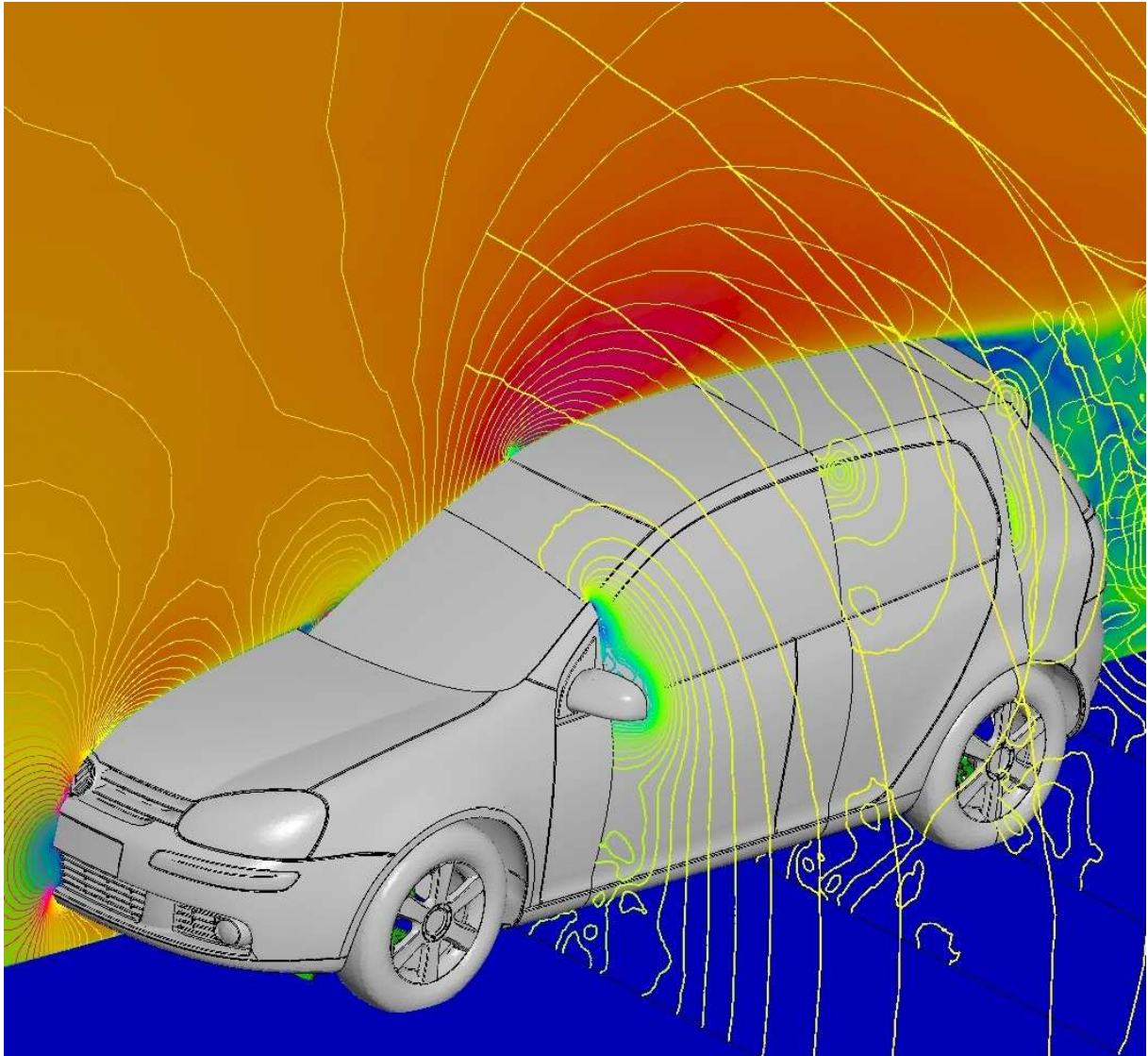


Figure 7p Pressure (Contours) and Velocity (Shaded) in Mid-Plane, Pressure (Contours) in x-Planes

The drag-coefficient obtained was $c_d = 0.309$, based on a reference velocity of $v_\infty = 33.33 \text{ m/s}$ and an area of $A = 2.2 \text{ m}^2$. Experiments conducted at VW measured a drag-coefficient of $c_d = 0.330$. However, the windtunnel model exhibited an open grille. From past experience, one can infer that performing the experiment with a closed front, as was done for the present run, would reduce the c_d by 5-10% percent in comparison with an open grille. At VW, the estimated value for the closed grille case was $c_d = 0.305$. The purely body-fitted CFD run with the same code yielded a drag-coefficient of $c_d = 0.320$. Overall, this leads us to conclude that with the present approach results within 5% of experimental values can be obtained, not bad considering the reduction in set-up times, and well within a range to make them of interest for designers. Moreover, as experience with this approach accumulates, we expect to be able to obtain even better results.



Figures 7q Velocities in Mid-Plane

V. CONCLUSIONS AND OUTLOOK

Body-fitted and embedded mesh techniques were combined to obtain accurate external aerodynamic solutions for realistic car geometries with minimal user intervention. The key idea is to mesh with typical body-fitted RANS grids the external shape of the vehicle, which is smooth and requires detailed physical modeling. The underhood and undercarriage are treated as embedded surfaces. The flow in this region is massively separated, requiring LES runs and isotropic grids. This makes it a suitable candidate for embedded grids.

Solutions have been obtained for a typical car geometry using this approach. Comparisons with body-fitted and experimental data show that this approach can yield drag predictions with an error less than 5%.

The great advantage seen in the present approach is that turnaround times for complete car geometries can be lowered to 1-2 days without compromising accuracy.

VI. ACKNOWLEDGEMENT

The authors wish to thank Volkswagen AG, Wolfsburg, Germany for providing the data of the VW GOLF 5 for testing this new approach. In particular we would like thank the 'Vehicle Development CAE-Methods' department at VW, especially Dr. Othmer for the useful discussions and exchange of ideas which were the starting point of this project.

References

- ¹M.J. Aftosmis, M.J. Berger and G. Adomavicius - A Parallel Multilevel Method for Adaptively Refined Cartesian Grids with Embedded Boundaries; *AIAA-00-0808* (2000).
- ²P. Angot, C.-H. Bruneau and P. Fabrie - A Penalization Method to Take Into Account Obstacles in Incompressible Viscous Flows; *Numerische Mathematik* 81, 497-520 (1999).
- ³J.D. Baum, H. Luo and R. Löhner - Numerical Simulation of a Blast Withing a Multi-Room Shelter; pp. 451-463 in *Proc. MABS-13 Conf.* The Hague, Netherlands, September (1993).
- ⁴J.D. Baum, H. Luo and R. Löhner - Numerical Simulation of Blast in the World Trade Center; *AIAA-95-0085* (1995).
- ⁵J.D. Baum, E. Mestreau, H. Luo, R. Löhner, D. Pelessone and Ch. Charman - Modeling Structural Response to Blast Loading Using a Coupled CFD/CSD Methodology; *Proc. Des. An. Prot. Struct. Impact/ Impulsive/ Shock Loads (DAPSIL)*, Tokyo, Japan, December (2003).
- ⁶Y. Cho, S. Boluriaan and P.J. Morris - Immersed Boundary Method for Viscous Flow Around Moving Bodies; *AIAA-06-1089* (2006).
- ⁷D.K. Clarke, H.A. Hassan and M.D. Salas - Euler Calculations for Multielement Airfoils Using Cartesian Grids; *AIAA-85-0291* (1985).
- ⁸A. Dadone and B. Grossman - An Immersed Boundary Methodology for Inviscid Flows on Cartesian Grids; *AIAA-02-1059* (2002).
- ⁹E.A. Fadlun, R. Verzicco, P. Orlando and J. Moud-Yusof - Combined Immersed-Boundary Finite-Difference Methods for Three-Dimensional Complex Flow Simulations; *J. Comp. Phys.* 161, 33-60 (2000).
- ¹⁰A. Gilmanov and F. Sotiropoulos - A Hybrid Cartesian/Immersed Boundary Method for Simulating Flows with 3-D, Geometrically Complex Moving Bodies; *J. Comp. Phys.* 207, 2, 457-492 (2005).
- ¹¹D. Goldstein, R. Handler and L. Sirovich - Modeling a No-Slip Flow Boundary with an External Force Field; *J. Comp. Phys.* 105, 354366 (1993).
- ¹²S.L. Karman - SPLITFLOW: A 3-D Unstructured Cartesian/ Prismatic Grid CFD Code for Complex Geometries; *AIAA-95-0343* (1995).
- ¹³J. Kim, D. Kim and H. Choi - An Immersed-Boundary Finite-Volume Method for Simulation of Flow in Complex Geometries; *J. Comp. Phys.* 171, 132-150 (2001).
- ¹⁴A.M. Landsberg and J.P. Boris - The Virtual Cell Embedding Method: A Simple Approach for Gridding Complex Geometries; *AIAA-97-1982* (1997).
- ¹⁵R.J. LeVeque and D. Calhoun - Cartesian Grid Methods for Fluid Flow in Complex Geometries; pp. 117-143 in *Computational Modeling in Biological Fluid Dynamics* (L. J. Fauci and S. Gueron, eds.), IMA Volumes in Mathematics and its Applications 124, Springer-Verlag (2001).
- ¹⁶R. Löhner and P. Parikh - Three-Dimensional Grid Generation by the Advancing Front Method; *Int. J. Num. Meth. Fluids* 8, 1135-1149 (1988).
- ¹⁷R. Löhner, P. Parikh and C. Gumbert - Some Algorithmic Problems of Plotting Codes for Unstructured Grids; *AIAA-89-1981-CP* (1989).
- ¹⁸R. Löhner and J.D. Baum - Adaptive H-Refinement on 3-D Unstructured Grids for Transient Problems; *Int. J. Num. Meth. Fluids* 14, 1407-1419 (1992).
- ¹⁹R. Löhner - Extensions and Improvements of the Advancing Front Grid Generation Technique; *Comm. Num. Meth. Eng.* 12, 683-702 (1996).
- ²⁰R. Löhner, Chi Yang, J. Cebal, O. Soto, F. Camelli, J.D. Baum, H. Luo, E. Mestreau, D. Sharov, R. Ramamurti, W. Sandberg and Ch. Oh - Advances in FEFLO; *AIAA-01-0592* (2001).
- ²¹R. Löhner, Chi Yang, J. Cebal, O. Soto, F. Camelli, J.D. Baum, H. Luo, E. Mestreau and D. Sharov - Advances in FEFLO; *AIAA-02-1024* (2002).
- ²²R. Löhner - Multistage Explicit Advective Prediction for Projection-Type Incompressible Flow Solvers; *J. Comp. Phys.* 195, 143-152 (2004).
- ²³R. Löhner, J.D. Baum, E. Mestreau, D. Sharov, C. Charman and D. Pelessone - Adaptive Embedded Unstructured Grid Methods; *Int. J. Num. Meth. Eng.* 60, 641-660 (2004).
- ²⁴R. Löhner and E. Oñate - A General Advancing Front Technique for Filling Space With Arbitrary Objects; *Int. J. Num. Meth. Eng.* 61, 1977-1991 (2004).
- ²⁵R. Löhner, J.D. Baum and E.L. Mestreau - Advances in Adaptive Embedded Unstructured Grid Methods; *AIAA-04-0083* (2004).
- ²⁶R. Löhner, Chi Yang, J.R. Cebal, F. Camelli, O. Soto and J. Waltz - Improving the Speed and Accuracy of Projection-Type Incompressible Flow Solvers; *Comp. Meth. Appl. Mech. Eng.* 195, 23-24, 3087-3109 (2006).
- ²⁷J.E. Melton, M.J. Berger and M.J. Aftosmis - 3-D Applications of a Cartesian Grid Euler Method; *AIAA-93-0853-CP* (1993).
- ²⁸R. Mittal and G. Iaccarino - Immersed Boundary Methods; *Annu. Rev. Fluid Mech.* 37, 239-261 (2005).
- ²⁹J. Mohd-Yusof - Combined Immersed-Boundary/B-Spline Methods for Simulations of Flow in Complex Geometries; *CTR Annual Research Briefs*, NASA Ames Research Center/ Stanford Univ., 317-327 (1997).
- ³⁰S.M. Murman, M.J. Aftosmis and M.J. Berger - Implicit Approaches for Moving Boundaries in a 3-D Cartesian Method; *AIAA-03-1119* (2003).
- ³¹R.B. Pember, J.B. Bell, P. Colella, W.Y. Crutchfield and M.L. Welcome - An Adaptive Cartesian Grid Method for Unsteady Compressible Flow in Irregular Regions; *J. Comp. Phys.* 120, 278 (1995).
- ³²C.S. Peskin - The Immersed Boundary Method; *Acta Numerica* 11, 479-517 (2002).

- ³³S. Del Pino and O. Pironneau - Fictitious Domain Methods and Freefem3d; *Proc. ECCOMAS CFD Conf.* , Swansea, Wales (2001).
- ³⁴J.J. Quirk - A Cartesian Grid Approach with Hierarchical Refinement for Compressible Flows; *NASA CR-194938, ICASE Report No. 94-51*, (1994).
- ³⁵H. Schlichting - *Boundary Layer Theory*; McGraw-Hill (1979).
- ³⁶R. Tilch and R. Löhner - Advances in Discrete Surface Grid Generation: Towards a Reliable Industrial Tool for CFD; *AIAA-02-0862* (2002).
- ³⁷PRE-FLOWTM2004 - Reference Manual©(PDF); *ESI Group*, (2004).
- ³⁸POST-FLOWTM2004 Reference Manual©(PDF); *ESI Group*, (2004).
- ³⁹PAM-FLOWTM2004 Reference Manual©(PDF)& User manual©(PDF); *ESI Group*, (2004).
- ⁴⁰D. de Zeeuw and K. Powell - An Adaptively-Refined Cartesian Mesh Solver for the Euler Equations; *AIAA-91-1542* (1991).